Materials and Design 195 (2020) 109022

Contents lists available at ScienceDirect

Materials and Design

journal homepage: www.elsevier.com/locate/matdes

# Optimization scheme of the orientation relationship from crystallographic statistics of variants and its application to lath martensite

Duanjun Sun [a], Chuanwei Li [b], Xuan Xue [b], Yi Liu [a], Zhenghong Guo [a,*], Jianfeng Gu [b,*]

[a] School of Materials Science and Engineering, Shanghai Jiao Tong University, Shanghai 200240, China
[b] Institute of Materials Modification and Modelling, Shanghai Jiao Tong University, Shanghai 200240, China

## HIGHLIGHTS

- This optimization scheme of determining the orientation relationship possesses a high accuracy with an error less than 1°, which was examined by the in-situ EBSD test.
- Without sacrificing any solution accuracy, a significant improvement of calculation efficiency was realized by this optimization scheme.
- This optimization scheme can effectively eliminate the influence of the random cross-sections on the actual orientation relationship.

## GRAPHICAL ABSTRACT

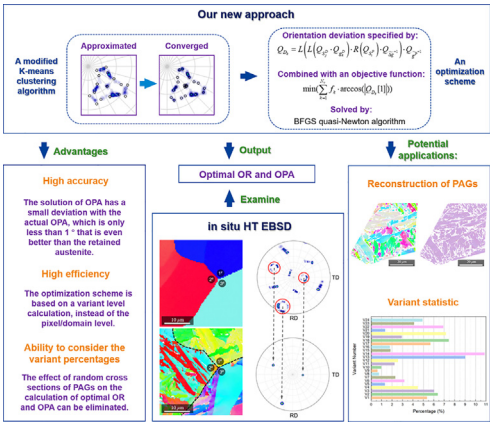


## ARTICLE INFO

*Article history:*
Received 7 July 2020
Accepted 31 July 2020
Available online 6 August 2020

*Keywords:*
Clustering algorithm
Optimization scheme
Orientation relationship
In-situ high temperature EBSD
Martensitic transformation

## ABSTRACT

Without sacrificing any solution accuracy, an efficient optimization scheme of determining the orientation relationship only based on the daughter phase (i.e., lath martensite in steels in this paper) was established in this work, which involves two key steps. Firstly, an accurate clustering algorithm was developed to perform a statistic of all variants, which can give the most probable orientation and area fraction for each variant. Different from previous methods, the second step is to perform a newly-established optimization scheme, which is able to take variant fractions into consideration to determine the optimal orientation relationship and orientation of prior austenite simultaneously. In this case, the variant-level calculation, which can save much computational time compared with pixel/domain-level calculation, is beneficial for the efficiency promotion. Through inputting the equally-weighted variants into the optimization scheme, the influence of the random cross-sections on the solutions can be effectively eliminated. Furthermore, in-situ high temperature EBSD examinations were first performed to validate solution accuracy, the corresponding results clearly indicated that the orientation of austenite obtained from this approach exhibited a high accuracy and the error is less than 1°.



* Corresponding authors.
*E-mail addresses:* zhenghongguo@sjtu.edu.cn (Z. Guo), gujf@sjtu.edu.cn (J. Gu).

https://doi.org/10.1016/j.matdes.2020.109022

## 1. Introduction

Among martensitic family, the lath martensite, which is formed in low carbon and low alloy steels, becomes the most preferred one in industrial applications due to its outstanding strength-toughness matching [1]. In fact, the excellent mechanical properties of lath martensite associated with its hierarchical configuration can be well-explained by the crystallographic theory which indicates that the minimum transformation strain plays a significant role [2]. However, the orientation relationship (OR) between prior austenite and lath martensite, as one of the critical parameters in crystallographic theory [3], is difficult to be measured accurately and conveniently by electron backscattering diffraction (EBSD) or even transmission electron microscopy (TEM) technique when the retained austenite can be found hardly in specimen. It includes two aspects. Firstly, some full-martensite steels contain hardly any retained austenite, which makes the characterization difficult [4,5]; Secondly, even if there is detectable amount of retained austenite in specimen, the serious strain due to martensitic transformation can cause the orientation deviation of untransformed austenite from the initial state [6], resulting in the unreliability of the OR measured from the EBSD or TEM examination after transformation.

To resolve these characterization problems, many methods are proposed to determine the OR only based on the martensitic variants within a prior austenite grain (PAG). An alternative method is to compare the well-documented ORs (e.g., K-S [7], N-W [8] or G-T relation [9,10]) with the measured one using stereographic projections on which the high-indexed directions are plotted [4,5]. Another automatic method was successfully applied in some cases [11−13]. It employs the well-documented ORs to calculate the "summation of mutual misorientation angle (SMMA)" with respect to each set of potential parent orientations, then the most probable OR and the parent orientation are determined with a minimum of SMMA. This method does not need any retained austenite and is sensitive to different ORs, however it is still semi-quantitative. Recently, several authors have proposed different quantitative methods to deduce a representative OR based on the EBSD data of only martensitic variants. Miyamoto et al. [6,14] presented a method determining both actual OR and orientation of prior austenite (OPA) through numerical fitting of EBSD data to minimize the average deviation between measured and predicted data of martensitic orientation. Although the criterion of minimization is quite reasonable, the least squares fitting method which they used is hard to obtain the optimal solution without numerical calculations. Later, Humbert et al. [15] proposed an analytical method with the advantage of rapid solution by introducing the quaternion algorithm into the procedure. Based on the Lagrange multiplier rule, this method is handled as an optimization scheme achieving the most concentrated orientation of calculated OPA, then the corresponding averaged OR is considered as the best representative solution. However, the definition of most concentrated orientation of calculated OPA deviates from the criterion of Miyamoto's method. After reviewing the details of these methods, in the present work, a robust minimization criterion which the variant fractions are introduced into is established. Our calculation is based on the variant-level data and thus need an ability of taking the variant proportions into consideration which is ignored in previous methods. And an objective function was also developed with quaternion facilities, which can be further solved using quasi-Newton method quickly.

Before applying our new approach to determine the optimal OR and OPA, two situations may draw attention from researchers. Since the normal EBSD is two-dimensional characterization technique, the area percentages of variants within the cross-section of a PAG are always not equal. In some cases, even the number of variants which can be detected may not reach the maximum (i.e., 24 for K-S/G-T OR and 12 for N-W OR) [16]. Under this situation, such an influence on the calculations should be considered. Another situation concerns on the computational efficiency, since it is quite time-consuming if we use pixel-level information to perform the calculation [17]. In the previous proposals, one alternative method is to use the averaged orientations of grains by adopting the classical grain detection algorithm [18]. However, it is inevitable that some information will be lost during averaging, which is damageable for the accuracy of the solutions [17]. With regard to the typical bivariant structure in lath martensite, the small misorientation between two different variants within a block and the orientation gradient within each variant can give rise to the result that these two variants are easily averaged into a single domain with a new orientation and which is, to some extent, not reliable or rigorous. For instance, averaging the orientations of these two variants with K-S or G-T OR leads to a new domain with N-W OR. Therefore, it seems that the previous proposals are difficult to balance the computational efficiency and solution accuracy. In order to escape from this dilemma, an available way is to perform a statistic of variants within each PAG before carrying out the optimization calculation of both OR and OPA. Since the number of variants is less than that of domains or pixels, the optimization calculation based on the variant-level consumes much less computational time. In the meantime, an appropriate method for variant statistics can also avoid any loss of orientation information effectively. In this work, the K-means clustering algorithm, as a basic algorithm of machine learning [19], is modified and employed to determine the orientation of each variant which is further applied to the area statistics of all variants. In addition, this new statistical method is also promising to be applied in the analysis of variant selection, which can provide the higher reliability than previous convenient method [20] relying on the well-documented ORs.

Although many different methods to determine the optimal OR and OPA were proposed, how to evaluate the accuracy of solutions is still an important and challenging issue. The previous works expected to evaluate it through the retained austenite [21], however, the disadvantages are still obvious, such as the orientation deviation of prior austenite caused by strain accommodation during martensitic transformation [6]. The present study intends to provide a more convincible and reasonable tool to resolve this issue, i.e., to compare the calculated solutions with the actual OPA (above $M_S$ temperature) obtained by in-situ high temperature (HT) EBSD examination. As far as the present authors are aware, the similar experimental verification has not been published by now. Besides that, based on the orientation change of prior austenite, the shear strain of retained austenite suffered from the surrounding martensite can be also estimated, which serves as an important parameter in the crystallographic theory of martensitic transformation.

## 2. Experimental procedures

A steel plate with a chemical composition Fe-12.75%Ni-1.518%Si-0.216%C (wt.%) was homogenized at 1473 K for 3 h, followed by water quenching to obtain the full lath martensite microstructure. Specimens cut from plate were mechanically grinded with SiC grid papers to remove the potential decarburization layer and then subjected to electropolishing process in a mixture solution of 7% perchloric acid and 93% ethanol at 243 K for 90 s to remove the possible damage layer at surface caused by the mechanical grinding. Then the EBSD measurements with a step size of 200 nm were performed using a SEM (LYRA3 GMU, TESCAN) equipped with an AZtecHKL EBSD system operated at 20 kV.

In order to evaluate the solution accuracy of present approach, an in-situ HT EBSD examination at elevated temperatures was also performed on other specimens with the same preparation procedure mentioned above. The specimen was firstly heated in the hot stage (Murano 525 with USB temperature controller, Gatan) to 750 °C and hold for 1.5 h to obtain the full-austenite microstructure, because $A_{c3}$ temperature of this steel is 688 °C. To avoid the effect of thermal radiation on the EBSD test, the specimen cooled down to a lower temperature of 320 °C which is still higher than the $M_S$ temperature of 225 °C to perform the HT EBSD examination. After that, the specimen was naturally cooled in the hot stage to room temperature, and the in-situ HT EBSD examination was performed again at the same position.

In addition, EBSD images displayed in this paper were created with HKL Channel5 EBSD software or matlab2018a software by programing. The MTEX 5.1.1 software [22] and PTClab software [23] were employed to plot pole figures (PFs). Moreover, a threshold value for the mean angular deviation (MAD) representing the fit goodness of the solution less than 0.8° was employed to avoid noise and "artificial" martensitic variants.

## 3. Methodologies

### 3.1. Preliminary analyses

Before detailing the new approach, some preliminary analyses are introduced firstly. Under the assumption of invariant plane strain, the martensite has a reproducible OR with respect to the prior austenite [24–26]. The OR between these two phases can be illustrated by the following equation:

$$\Delta g \cdot S_i^P \cdot g^P = S_j^D \cdot g^D \tag{1}$$

where superscripts $P$ and $D$ indicate the parent and daughter phase respectively; $S$ with subscripts $i$ or $j$ means the $i^{th}$ or $j^{th}$ rotational symmetry element; $\Delta g$ indicates the OR associating the orientations of parent phase ($g^P$) with that of the daughter phase ($g^D$). Particularly, orientations of $g^P$ and $g^D$ make the sample reference frame parallel to that of the cubic crystals. For cubic lattice systems, the orientation of daughter variant can be given by Eq. (2) after a simple transposition on Eq. (1):

$$g^D = \left(S_j^D\right)^{-1} \cdot \Delta g \cdot S_i^P \cdot g^P = S_k^D \cdot \Delta g \cdot S_i^P \cdot g^P \tag{2}$$

where $k$ also means the $k^{th}$ rotational symmetry element. The reason why the second equal sign is established is that the symmetric element set with respect to cubic crystal system is closed to the inversion operation. According to this equation, it is true that: i) each symmetry element of $S_i^P$ corresponds to a specific orientation of variant, which indicates that all potential orientations of variants can be deduced if the orientation of parent phase is given; ii) the number of variants depends on the term of $\Delta g \cdot S_i^P$, which can only less than or equal to the number of the total symmetry element of parent phase (i.e., 24/24/12 for K-S/G-T/N-W OR). For lath martensite case, three well-documented ORs and their stereographic PFs are shown in Table 1 and Fig. 1 respectively.

Among these ORs, K-S and N-W have exact low-index parallelism between direction and plane respectively, while the G-T OR is usually expressed by approximate match and a frequently used one has the form with high-index relation: $\{111\}_\gamma//\{011\}_{\alpha'}$ and $<5\ 12\ 17>_\gamma//<7\ 17\ 17>_{\alpha'}$ [5,27]. It follows that these three sets of ORs are related by a rotation less than 5.26° about the normal of $\{111\}_\gamma//\{110\}_{\alpha'}$ plane, indicating the quite similar ORs. Nevertheless, a pronounced distinction can be observed through $\{001\}_\gamma$ standard stereographic projections on which the high-index directions of martensite are plotted.

**Table 1**
The orientation relationship matrix between prior austenite and martensite.

| Name | OR | Orientation relationship matrix |
|---|---|---|
| K-S [7] | $\{111\}_\gamma//\{110\}_{\alpha'}$, $\langle 110\rangle_\gamma//\langle 111\rangle_{\alpha'}$ | $\begin{pmatrix} 0.7416 & -0.6667 & -0.0749 \\ 0.6498 & 0.7416 & -0.1667 \\ 0.1667 & 0.0749 & 0.9832 \end{pmatrix}$ $(111)_\gamma//(011)_{\alpha'}$ $[-101]_\gamma//[-1-11]_{\alpha'}$ |
| N-W [8] | $\{111\}_\gamma//\{110\}_{\alpha'}$, $\langle 112\rangle_\gamma//\langle 110\rangle_{\alpha'}$ | $\begin{pmatrix} 0.7071 & -0.7071 & 0 \\ 0.6969 & 0.6969 & -0.1691 \\ 0.1196 & 0.1196 & 0.9856 \end{pmatrix}$ $(111)_\gamma//(011)_{\alpha'}$ $[-1-12]_\gamma//[0-11]_{\alpha'}$ |
| G-T [5,27] | $\{111\}_\gamma//\{110\}_{\alpha'}$, $<5\ 12\ 17>_\gamma//<7\ 17\ 17>_{\alpha'}$ | $\begin{pmatrix} 0.7266 & -0.6859 & -0.0407 \\ 0.6716 & 0.7215 & -0.1684 \\ 0.1449 & 0.095 & 0.9849 \end{pmatrix}$ $(111)_\gamma//(011)_{\alpha'}$ $[-12-5\ 17]_\gamma//[-7-17\ 17]_{\alpha'}$ |

Furthermore, given the orientation of daughter phase, the orientation of parent phase can be deduced by Eq. (3):

$$g^P = \left(\Delta g \cdot S_i^P\right)^{-1} \cdot S_j^D \cdot g^D = S_l^P \cdot (\Delta g)^{-1} \cdot S_j^D \cdot g^D \tag{3}$$

where $l$ also means the $l^{th}$ rotational symmetry element. Let us review the ideal situation where the standard K-S, N-W and G-T ORs are taken into consideration. There are 24 distinct OPA with respect to both K-S and G-T OR, but the number is reduced to 12 for N-W OR in that half of them are repetitive due to the particularity of N-W OR. Moreover, it should be clear that only one variant is not enough to obtain the unique solution of OPA, but we can find their intersection of potential sets of OPA calculated from two distinct variants to get access to the authentic OPA. Referring to the previous variant labels [27–29], Table 2 lists the potential OPA deduced from the orientations of arbitrary two variants in the case of K-S, N-W and G-T ORs respectively, where matrix $g^{P0}$ indicates the authentic OPA, and the other potential OPA can be represented by $(T \cdot g^{P0})$.

Apparently, there exist some limited combinations of two distinct variants that can determine the authentic OPA. Besides, the matrix $T_1$ is a reflection operation about $(111)_\gamma$ plane superimposed with an inversion operation, it follows that the OPA deduced from all variants from a packet (for K-S/G-T/N-W ORs) should have two solutions with mirror symmetry (the inversion operation is not considered because it is one of the symmetry operations with respect to the cubic lattice system). As shown in Fig. 1d, the PAG and its twin have six variants which have the same orientations. Accordingly, if variants are selected randomly, the minimum number that is sufficient to determine authentic OPA is 7, 7 and 4 for K-S, G-T and N-W OR respectively. However, the number can be reduced to 3, 2 and 3 if variants are selected from different packets. Furthermore, variants within a PAG can be divided into three Bain groups, and misorientation between any two variants in the same Bain group is within ~15°. Due to high orientation scatter in the measured data, such small misorientation leads to a difficulty in discriminating the potential OPAs of variants from the same Bain group. To improve the accuracy of initial OPA, it is recommended that three different variants from different Bain groups in different packets together serve as the necessary candidates.

When it comes to the practical measurements, authentic OPAs deduced from different variants cannot match perfectly since the orientation scatter of variants always leads to deviations from the ideal orientation (e.g., Fig. 3b), which therefore needs special consideration. In fact, such a situation can be divided into two cases described in the following section, depending on whether the OR can be approximately estimated.

### 3.2. Pre-approximated OR and OPA

*Case 1: the OR can be approximately estimated.*

For lath martensite, the OR can always be estimated through comparing the measured stereographic projection with the well-documented ORs. Given the approximated OR, all potential OPAs can be deduced from Eq. (3). Indeed, according to the analysis from Table 2, a schematic diagram (see Fig. 2) illustrates that the authentic OPA needs to satisfy two conditions: 1) the cluster of potential OPAs has the highest orientation intensity, and 2) the number of potential OPAs of cluster is equal to that of the involved variants.

Based on the pre-analysis mentioned above, a simple algorithm is developed to approximate the authentic OPA, which is given by the following procedures:

(i) Any three different variants from different Bain groups respectively are selected out. This can be achieved by the criterion that the misorientation between any two of them is about 60°.
(ii) 72 (=24 × 3) potential OPAs can be obtained according to Eq. (3). And then, check whether there are three OPAs satisfying a condition that the misorientation between any two of them is

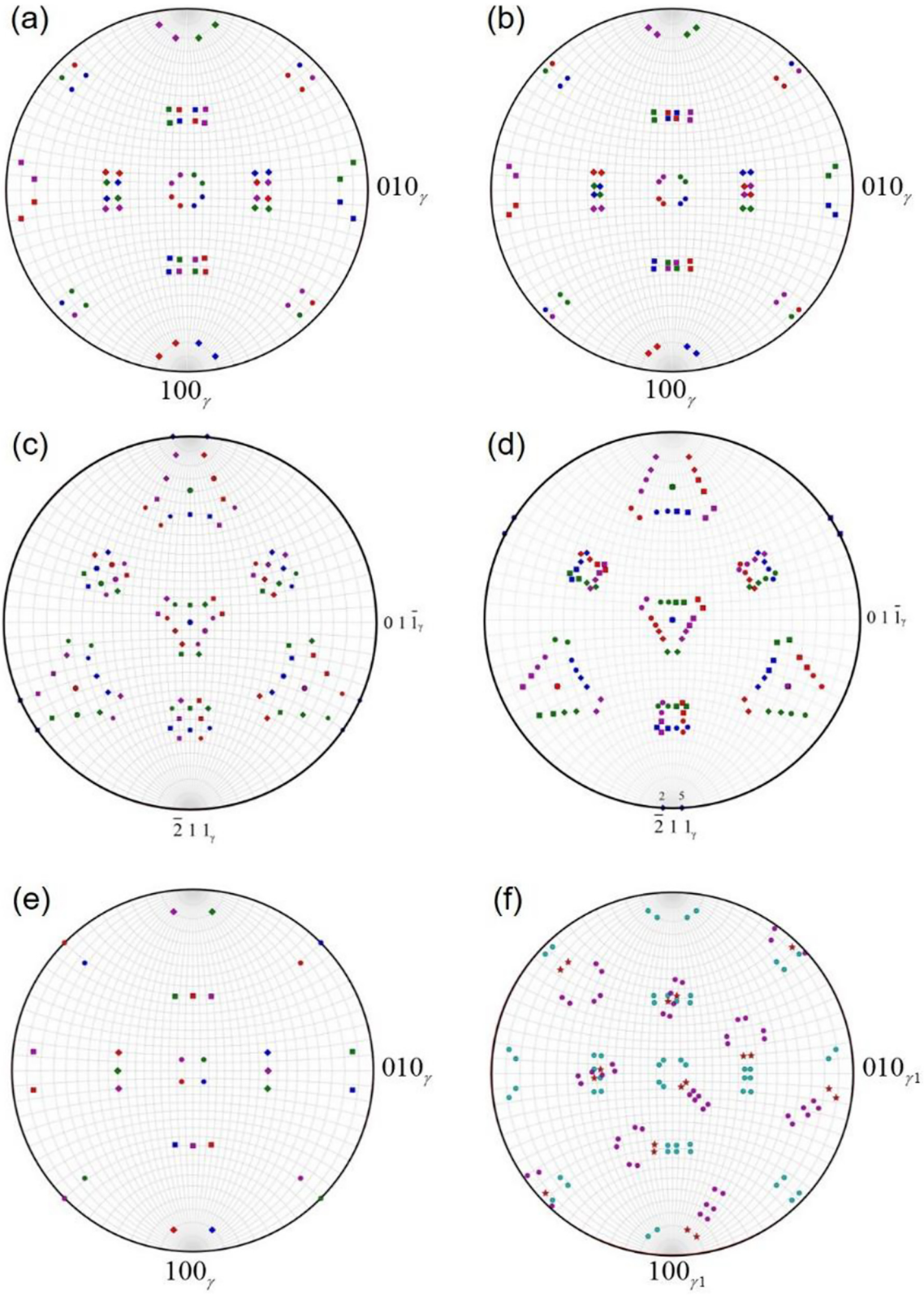


**Fig. 1.** Standard $\{001\}_{\alpha'}$ pole figures (PFs) for variants with K-S (a), G-T (b) and N-W (e) ORs and $\{011\}_{\alpha'}$ PFs for variants with K-S (c), G-T (d), where the poles of variants with the same color or the same shape indicate the same packet group or the same Bain group respectively. (f) A prior austenite grain and its twin have six variants with common orientation marked as red stars, taking G-T OR as an example.

less than a critical value, where 10° is recommended since the growth of martensite single crystal cannot be hindered by small angle boundary effectively. If it does, the averaged orientation of these three potential OPAs can be presented as the orientation of this cluster which can be further treated as the approximated OPA.

(iii) However, there may be more than one cluster in practical measurement. For these three OPAs of a cluster whose

**Table 2**
Potential OPA deduced from the orientations of two distinct variants with K-S, N-W or G-T ORs respectively.

| Variant pair | K-S OR | G-T OR | N-W OR |
|---|---|---|---|
| V1/V2 | $g^{P0}$; $T_1{\cdot}g^{P0}$; $T_2{\cdot}g^{P0}$; $T_3{\cdot}g^{P0}$; $T_4{\cdot}g^{P0}$ | $g^{P0}$; $T_1{\cdot}g^{P0}$ | $g^{P0}$; $T_1{\cdot}g^{P0}$ |
| V1/V3 | $g^{P0}$; $T_1{\cdot}g^{P0}$; $T_5{\cdot}g^{P0}$; $T_6{\cdot}g^{P0}$ | $g^{P0}$; $T_1{\cdot}g^{P0}$; $T_7{\cdot}g^{P0}$; $T_8{\cdot}g^{P0}$ | $g^{P0}$; $T_1{\cdot}g^{P0}$ |
| V1/V4 | $g^{P0}$; $T_1{\cdot}g^{P0}$ | $g^{P0}$; $T_1{\cdot}g^{P0}$ | $g^{P0}$; $T_9{\cdot}g^{P0}$ |
| V1/V5 | $g^{P0}$; $T_1{\cdot}g^{P0}$; $T_5{\cdot}g^{P0}$ | $g^{P0}$; $T_1{\cdot}g^{P0}$; $T_7{\cdot}g^{P0}$; $T_8{\cdot}g^{P0}$ | $g^{P0}$ |
| V1/V6 | $g^{P0}$; $T_1{\cdot}g^{P0}$ | $g^{P0}$; $T_1{\cdot}g^{P0}$ | |
| V1/V7 | $g^{P0}$; $T_3{\cdot}g^{P0}$; $T_4{\cdot}g^{P0}$ | $g^{P0}$ | |
| V1/V8 | $g^{P0}$; $T_3{\cdot}g^{P0}$; $T_4{\cdot}g^{P0}$ | | |
| V1/V9 | $g^{P0}$ | | |
| V1/V10 | | | |
| V1/V11 | | | |
| V1/V12 | | | |
| V1/V13 | | | – |
| V1/V14 | | | |
| V1/V15 | | | |
| V1/V16 | | | |
| V1/V17 | | | |
| V1/V18 | | | |
| V1/V19 | | | |
| V1/V20 | | | |
| V1/V21 | | | |
| V1/V22 | | | |
| V1/V23 | | | |
| V1/V24 | | | |
| Remarks | $T_1=\begin{pmatrix}-0.3333 & 0.6667 & 0.6667\\ 0.6667 & -0.3333 & 0.6667\\ 0.6667 & 0.6667 & -0.3333\end{pmatrix}$ | $T_2=\begin{pmatrix}-0.9916 & -0.1292 & 0.0084\\ -0.1292 & 0.9832 & -0.1292\\ 0.0084 & -0.1292 & -0.9916\end{pmatrix}$ | $T_3=\begin{pmatrix}0.2500 & 0.6124 & -0.7500\\ -0.6124 & -0.5000 & -0.6124\\ -0.7500 & 0.6124 & 0.2500\end{pmatrix}$ |
| | $T_4=\begin{pmatrix}0.2500 & -0.6124 & -0.7500\\ 0.6124 & -0.5000 & 0.6124\\ -0.7500 & -0.6124 & 0.2500\end{pmatrix}$ | $T_5=\begin{pmatrix}0.0999 & -0.9888 & -0.1111\\ -0.9888 & -0.1111 & 0.0999\\ -0.1111 & 0.0999 & -0.9888\end{pmatrix}$ | $T_6=\begin{pmatrix}-0.7666 & 0.3221 & -0.5556\\ 0.3221 & -0.5556 & -0.7666\\ -0.5556 & -0.7666 & 0.3221\end{pmatrix}$ |
| | $T_7=\begin{pmatrix}0.0559 & -0.9967 & -0.0592\\ -0.9967 & -0.0592 & 0.0559\\ -0.0592 & 0.0559 & -0.9967\end{pmatrix}$ | $T_8=\begin{pmatrix}-0.7226 & 0.3300 & -0.6074\\ 0.3300 & -0.6074 & -0.7226\\ -0.6074 & -0.7226 & 0.3300\end{pmatrix}$ | $T_9=\begin{pmatrix}0 & 0.7071 & 0.7071\\ -0.7071 & 0.5000 & -0.5000\\ -0.7071 & -0.5000 & 0.5000\end{pmatrix}$ |

orientations are expressed by quaternions, the norm of the sum of those quaternions can be estimated as the intensity of this cluster [15]. And the cluster with the highest intensity is treated as the optimal solution.

*Case 2: no information about the OR.*

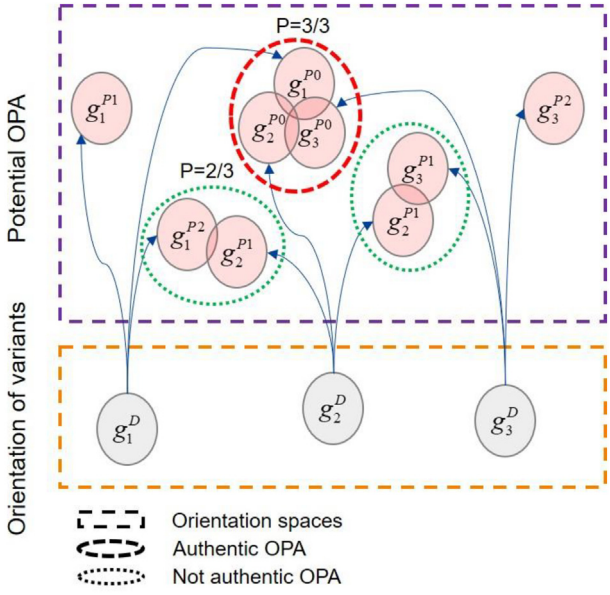


**Fig. 2.** The schematic diagram (adapted from Ref. [21]) illustrating the difference between the authentic orientation of prior austenite (OPA) and the other OPAs. P equals to the number of potential OPAs in a cluster over the number of variants involved.

When it comes to a special situation that the OR cannot be easily estimated, a method named by its creators Humbert et al. [30], XABX, is available. In this method, an error function which represents the misorientation between three potential OPAs to some extent is developed. With the only input of orientations of two variants within a PAG, an analytical solution is provided to minimize the error function. In order to match the notations and formulas in the present paper, a slightly modified version is briefly illustrated in the *Appendix A*, while the detailed description can be referred to Ref. [30].

Although the XABX method only uses the orientations of variants as the known condition without any information about the OR, it is still regarded as an approximate method. The reasons include: i) the proportion of variants on the optimal OR is not taken into account; ii) this method is established with a hypothesis that the OPAs do not vary with respect to different variants taken into calculation. Apparently, it is not easy to realize since the boundaries with small angles always exist in many practical cases; iii) Instead of all variants, the OR calculation involves only three neighboring ones within a PAG.

Based on the above summary of previous achievements, both OPA and OR can be roughly estimated. However, the OR is not only an essential parameter in the crystallographic theory, but also can have an influence on the mechanical properties. It follows that an accurate measurement of OR is required and of significance, and as shown in the following sections, our new approach is developed for this purpose.

### 3.3. Crystallographic statistics of variants

As we know, the specific OR is rarely maintained strictly within a PAG [31], a slight OR deviation usually occurs at different positions. In practical two-dimensional EBSD measurements, the area fractions of different variants vary greatly even in the un-deformed PAG. However, there is no reason for variant selection during the martensitic transformation in naturally quenched specimens. Therefore, the area factor

needs to be eliminated when performing the calculation for optimal OR and OPA, which can be realized by carrying out the variant statistic in advance.

Clustering is a machine learning technique that involves the grouping of data points. In the present section, the K-means clustering algorithm is modified and employed to the variant statistic, and quaternions are used to perform the algorithm. Correspondingly, the conversion formulas between rotation matrix and quaternion are listed in the *Appendix B*.

(i) The number of clusters (i.e., the value of K) is determined at first. According to the approximated OR, this number should be 24 in almost all cases with respect to lath martensite because only strict N-W OR can have 12 variants.

(ii) The centers of clusters should be initialized. Given the approximated OR and OPA, the orientation of variants can be obtained by Eq. (2), which can serve as the initial centers of clusters.

(iii) Each pixel data is classified by calculating the misorientation between this pixel and each center of clusters, and then classifying the pixel into the cluster whose center is the closest to it. Furthermore, a pixel whose orientation differs by more than a threshold value (10° in this paper) from that of the closest center of clusters will not be grouped into any clusters, this extra modification on the K-means clustering algorithm is to estimate the number of variants.
In this step, two essential calculations are involved. One is that the rotation angle with respect to a quaternion of $Q$ can be obtained by $2\arccos(Q[1])$ where $Q[1]$ is the first component of $Q$. The other is the misorientation calculation, which involves the quaternion multiplication. According to the multiplication rules [32], the $P\cdot Q$ representing a product of unit quaternions $P=[p_0,p_1,p_2,p_3]^T$ and $Q=[q_0,q_1,q_2,q_3]^T$ can be alternatively expressed by $L(P)\cdot Q$ or $R(Q)\cdot P$, where $L(P)$ and $R(Q)$ transform the quaternion form of $P$ and $Q$ into the matrix form:

$$L(P)=\begin{bmatrix} p_0 & -p_1 & -p_2 & -p_3 \\ p_1 & p_0 & -p_3 & p_2 \\ p_2 & p_3 & p_0 & -p_1 \\ p_3 & -p_2 & p_1 & p_0 \end{bmatrix} \quad (4-1)$$

$$R(Q)=\begin{bmatrix} q_0 & -q_1 & -q_2 & -q_3 \\ q_1 & q_0 & q_3 & -q_2 \\ q_2 & -q_3 & q_0 & q_1 \\ q_3 & q_2 & -q_1 & q_0 \end{bmatrix} \quad (4-2)$$

(iv) The center of each cluster is replaced by the averaged orientation of these classified pixels, and the averaged orientation from $N$ pixels is given by the following Eq. [33]:

$$Q_{\text{ave}}=\sum_{i=1}^{N} Q_i \Big/ \left\| \sum_{i=1}^{N} Q_i \right\| \quad (i=1,2,3,\ldots N) \quad (5)$$

where $Q_i$ indicates the quaternion of the orientation of the $i^{\text{th}}$ pixel data. One should be aware of that a three-dimensional rotation is represented by two opposite quaternions, and only the appropriate one (i.e., the orientation quaternions should have a same direction) should be selected during this averaging calculation.

(v) Repeat above steps until the centers of clusters barely change between two successive iterations. Here, the convergence criterion is that the misorientation of every cluster center between two successive iterations is less than 0.01°. After finishing the convergence, if there is any cluster which almost no pixels are grouped into, the value where K subtracts the number of the empty cluster stands for the number of variants.

After clustering, the area fraction of variants can be estimated through the number of pixels in every cluster since each pixel has the same area. Furthermore, the crystallographic statistics of variants allow the variant-level optimization of OR and OPA which can save computational time significantly because the number of variants is much lower than that of pixels or domains.

### 3.4. A robust optimization scheme for OR and OPA

Different from the previous method, the present solution of OR and OPA with consideration of the variant proportions is treated as an optimization scheme and can be solved by BFGS quasi-Newton algorithm [34] quickly. Firstly, an objective function needs to be built. After a simple transposition on Eq. (1), an orientation deviation between the measured and the predicted variants can be established:

$$D_m=\left[S_j^D\cdot g_m^D\right]\cdot\left[\widetilde{\Delta g}^{-1}\cdot S_i^P\cdot\widetilde{g^P}^{-1}\right] \quad (6)$$

where the subscript $m$ indicates the $m^{\text{th}}$ variant, $\widetilde{\Delta g}$ and $\widetilde{g}^P$ represent the predicted OR and parent orientation respectively. Before performing the new algorithm, if the symmetric elements of daughter and parent phases can be determined in advance, a large amount of computation costs can be saved. Fortunately, after substituting the inverse of the approximated OR and OPA for $\widetilde{\Delta g}^{-1}$ and $\widetilde{g}^{P^{-1}}$ respectively, it can be achieved when the rotation angle with respect to $D$ reaches a minimum value.

Due to the quaternion facilities, it is beneficial to transform Eq. (6) into quaternion form:

$$Q_{D_m}=\left[Q_{S_j^D}\cdot Q_{g_m^D}\right]\cdot\left[Q_{\Delta g^{-1}}\cdot Q_{S_i^P}\cdot Q_{g^{P-1}}\right] \quad (7)$$

Thanks to these two equivalent multiplications as shown in Eq. (4), the quaternion multiplication can be transformed into matrix form as shown in the following:

$$Q_{D_m}=L\left(L\left(Q_{S_j^D}\cdot Q_{g_m^D}\right)\cdot R\left(Q_{S_i^P}\right)\cdot Q_{\Delta g^{-1}}\right)\cdot Q_{g^{P-1}} \quad (8)$$

where the predicted $Q_{\widetilde{\Delta g}^{-1}}$ and $Q_{\widetilde{g^P}^{-1}}$ can be given by two undetermined quaternions $\left[\sqrt{1-{x_1}^2-{x_2}^2-{x_3}^2},x_1,x_2,x_3\right]$ and $\left[\sqrt{1-{x_4}^2-{x_5}^2-{x_6}^2},x_4,x_5,x_6\right]$ respectively whose first components implicates the constrain of unit quaternions. Besides that, due to the flexibility of equivalent multiplications, Eq. (8) gives only one form of the orientation deviations.

Finally, the objective function is specified by:

$$\min\left(\sum_{m=1}^{N_v} f_m\cdot\ \arccos\left(\left|Q_{D_m}[1]\right|\right)\right) \quad (9)$$

where $N_v$ is the number of variants, $f_m$ is the fraction of the $m^{\text{th}}$ variant, and $Q_{D_m}[1]$ indicates the first component of $Q_{D_m}$. In order to minimize the objective function given by Eq. (8) and (9), the current solution can be quickly solved by BFGS quasi-Newton method with inputting the initial value of $Q_{\widetilde{\Delta g}^{-1}}$ and $Q_{\widetilde{g^P}^{-1}}$ which the inverse of the approximated OR and OPA can respectively serve as.

Based on the optimal orientation of each variant after a clustering statistic, the new robust algorithm, which is viewed as an optimization scheme taking the proportion of variants into consideration, differs greatly from previous attempts proposed by other authors.

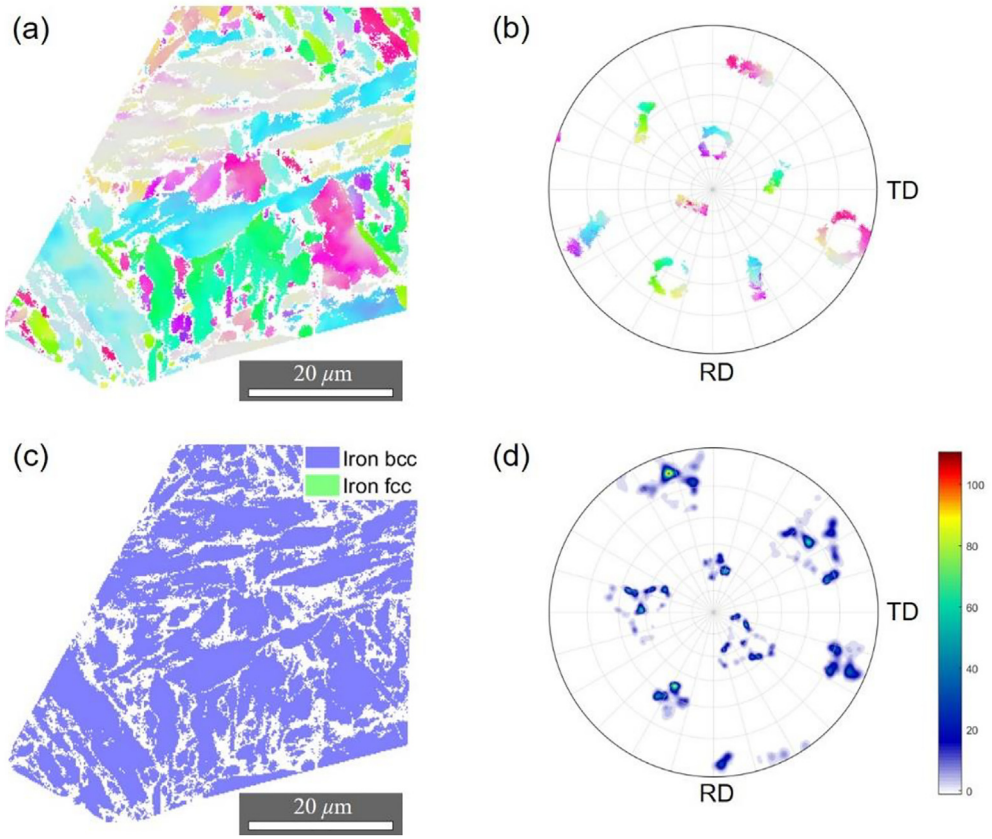


**Fig. 3.** The EBSD maps of the full martensite microstructure and its stereographic pole figures within a prior austenite grain. (a) Inverse pole figure (IPF) map of lath martensite; (b) {001} pole figure of lath martensite displayed as points; (c) Phase map of iron BCC and FCC, indicating no retained austenite; (d) {011} pole figure of lath martensite displayed as a contour. (For interpretation of the references to color in this figure legend, the reader is referred to the Web version of this article.)

## 4. Results

### *4.1. Application to a full-martensite microstructure at room temperature*

Following the algorithm developed above, the new approach to determine the optimal OR and OPA was applied to a steel with full-martensite microstructure at first.

A typical microstructure of full martensite is presented in Fig. 3a, which contains almost no retained austenite as shown in Fig. 3c. This is exactly the situation where the OR is difficult to be measured by the traditional EBSD technique but is available by the present approach. Compared with Fig. 1 and the martensite's {001} stereographic PF displayed as points (Fig. 3b), it is confirmed that the PAG contains 24 variants, indicating 24 clusters of variant orientations. Furthermore, in order to test the accuracy of the variant orientations that we estimated, a {011} stereographic PF with higher index plotted as a contour (Fig. 3d) is recommended since it shows the measured intensity of martensite.

In order to accelerate the convergence of clustering algorithm, the approximated OPA and OR were firstly employed to generate the initial value of the variant orientations. As shown in Fig. 4a, the approximated orientations of variants and the measured data do not match well. After transforming the orientation data into quaternion form, the modified K-means clustering algorithm was performed successfully. The desired convergence was quickly achieved with only 5 iterations, and the clustering results for each iteration are also provided in *Supplementary Movie* S1. It is clear that the variant orientation with respect to the converged results is almost perfect in accordance with the measured data as shown in Fig. 4b, indicating a high accuracy of this algorithm.

Based on the orientations of variants with respect to the converged and approximated results, the percentage of every variant was further calculated as shown in Table 3. When the converged result serves as the true value, the relative error of the approximated result varies from zero to a maximum value of 30.78%, indicating that the clustering algorithm is necessary to improve accuracy significantly. The image distribution of variants within the PAG are visualized in Fig. 5. It is a typical three-tier hierarchical configuration, where a PAG is composed of four crystallographically distinct packets, each of which consists of three blocks that exhibit a bivariant structure with V1/V4 pairs. This is consistent with previous studies on lath martensite [4,35]. From these results, the additional benefits of high accuracy from the present approach can even be extended to the identification of variant selection more easily during stress/strain induced martensitic transformation.

After obtaining the most representative orientations of variants with their area percentages, the robust algorithm of calculating the optimal OR and OPA was further performed by considering the proportions of variants (both area-weighted and equally-weighted), and the results are listed in Table 4. Here, the criterion judging the accuracy of solutions is specified by the following equation, which is similar with the criterion proposed by Miyamoto [6,14]:

$$\sum_{m=1}^{N_v} f_m \cdot \Delta\theta_m \tag{10}$$

where $\Delta\theta_m$ is the deviation between the measured and predicted data of the $m^{\text{th}}$ orientation of variant. Besides, the variant fraction, $f_m$, equals to $1/N_v$ for the equally-weighted case. For comparison, the variant orientation after clustering was also inputted into Humbert's method in Ref. [15], whose solution is also listed in Table 4. Apparently, the deviation of our solution is smaller, which indicates the better accuracy. In addition, there are only small misorientations between the optimal results

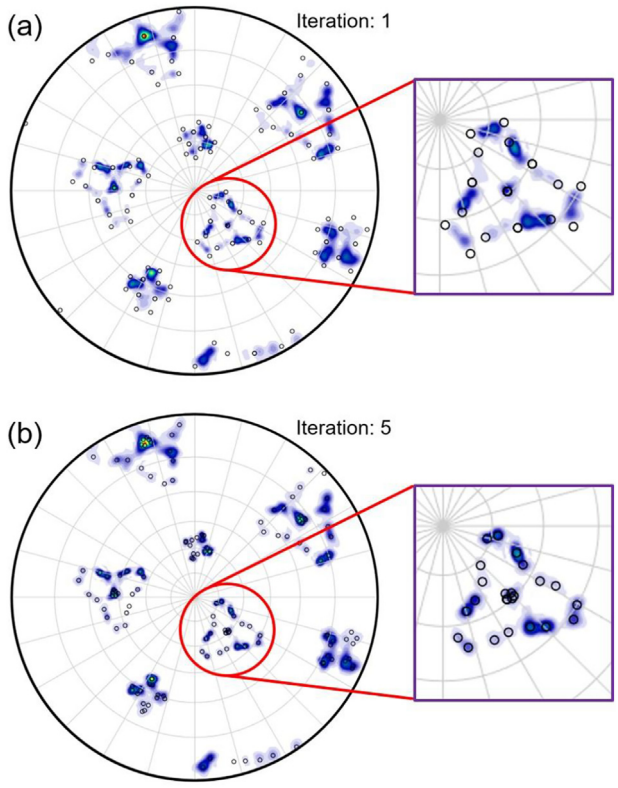


**Fig. 4.** The contoured {011} pole figure of lath martensite within the prior austenite grain in Fig. 3a superimposed onto the {011} pole figure of the calculated orientations of variants during the clustering. (a) and (b) show the first and the last iteration respectively.

(i.e., OR and OPA) solved by our and Humbert's approaches. Nevertheless, as is well known that the OR plays an essential role in the crystallographic theory, a small change in OR may imply a different mechanism of martensitic transformation [2,24], which thus deserves a rigorous treatment. Furthermore, as analyzed above, the optimal OR with equal area-weighted variants should be the solution for the present study, although whose deviation is slightly larger. This OR differs from G-T, N-W and K-S ORs by 1.63°, 2.45° and 3.54° respectively, suggesting that the G-T is the nearest OR in the specimen, and the angles between close-packed planes and close-packed directions are 1.39° and 3.29° respectively.

**Table 3**
The area percentage of variants with respect to the converged result (CR) and approximated result (AR) and the corresponding relative error.

| | | | | | | | | |
|---|---|---|---|---|---|---|---|---|
| Packet 1 | Variant | | V1 | V2 | V3 | V4 | V5 | V6 |
| | Area Percentage (%) | CR | 0.41 | 2.11 | 0.43 | 0.14 | 1.87 | 1.99 |
| | | AR | 0.41 | 1.80 | 0.52 | 0.14 | 2.15 | 1.90 |
| | Relative error (%) | | 0.00 | 14.65 | 20.54 | 0.00 | 15.32 | 4.45 |
| Packet 2 | Variant | | V7 | V8 | V9 | V10 | V11 | V12 |
| | Area Percentage (%) | CR | 12.26 | 1.08 | 6.40 | 10.96 | 1.57 | 9.73 |
| | | AR | 12.24 | 1.05 | 6.63 | 10.82 | 1.61 | 9.60 |
| | Relative error (%) | | 0.19 | 2.80 | 3.67 | 1.25 | 1.92 | 1.41 |
| Packet 3 | Variant | | V13 | V14 | V15 | V16 | V17 | V18 |
| | Area Percentage (%) | CR | 5.10 | 1.44 | 3.50 | 9.34 | 0.80 | 4.72 |
| | | AR | 5.69 | 1.35 | 3.71 | 8.75 | 0.89 | 4.69 |
| | Relative error (%) | | 11.58 | 5.83 | 5.98 | 6.32 | 10.12 | 0.74 |
| Packet 4 | Variant | | V19 | V20 | V21 | V22 | V23 | V24 |
| | Area Percentage (%) | CR | 3.61 | 1.64 | 3.13 | 15.00 | 1.04 | 1.71 |
| | | AR | 4.72 | 1.57 | 3.15 | 13.79 | 1.12 | 1.69 |
| | Relative error (%) | | 30.78 | 4.24 | 0.60 | 8.05 | 7.61 | 1.09 |

To verify the reliability of the solution further, the PAG was reconstructed based on a simple algorithm described in Appendix C as well, and the corresponding results are presented in Fig. 6. The stereographic PF of the reconstructed prior austenite (Fig. 6d) shows a good fitting with that of the measured variants (Fig. 6b), which indicates that the OR and OPA determined by the present approach are accurate and may be even propitious to the reconstruction of PAGs.

## 5. In-situ HT EBSD examination

In order to provide a relatively convincible examination to assess the solution accuracy, an in-situ HT EBSD analysis was performed to obtain the crystallographic data of prior austenite before martensitic transformation.

As presented in Fig. 7a, three austenite grains with a triple junction was observed at 320 °C (above $M_S$ temperature). While Fig. 7b and c shows the in-situ image at room temperature after specimen was cooled down naturally in the SEM chamber. There is a small amount of retained austenite dispersed among martensitic variants in each PAG. Furthermore, the stereographic PF of martensite within the first PAG labeled in Fig. 7c is also presented in Fig. 7d. The orientation scatter of variants is pronounced compared to those in the water-quenched specimen shown in above figures, which may bring challenges to the clustering procedure. Here, the averaged orientation of austenite grain at 320 °C will be the evaluation criterion for our calculated solution (i.e., OPA), while the orientation of retained austenite will be employed as a comparative data for illustrating the accuracy of our approach further.

After performing the clustering algorithm, the orientations of variants calculated show a good agreement with that of the experimental data, as revealed in the stereographic PF of martensite where the PF of the clustered variant orientations are superimposed (Fig. 8a). In addition, the area statistic of variants is also provided in Fig. 8b, which will be employed to the optimization scheme for OR and OPA.

Based on the clustered orientation of variants with their corresponding area percentages, the robust optimization scheme for OR and OPA was carried out. With respect to the first austenite grain, Table 5 shows that the OPA obtained from the present approach, no matter whether the area-weighted or the equally-weighted factor is involved, has a good agreement with the averaged austenite orientation obtained at 320 °C (with a misorientation less than 1°). However, the averaged orientation of all retained austenite within the first grain shows a misorientation of 1.43°, and this number will be even as large as 3.73° when averaging the misorientations between the austenite orientation at each pixel and the initial averaged orientation. This orientation change may be an inevitable result of the strain accommodation due to martensitic transformation, which leads to the unreliability when employing the retained austenite to serve as the prior austenite at elevated temperature. Therefore, the solution obtained by the present approach exhibits an even higher accuracy than using the orientation of retained austenite.

In addition, the method developed by Humbert et al. [15] was not suitable for dealing with this case because several eigenvalues of the matrix $A^TA$ (which is given in Ref. [15]) have the relatively high similarity, which may be caused by the orientation scatter of variants. Therefore, our approach is more robust, and it is believed that a higher solution accuracy can be achieved with respect to the water-quenched microstructure, since a much less orientation scatter of variants is observed compared to the specimen natural-cooled in the SEM chamber.

## 6. Discussions

Due to the small difference among the well-documented ORs (e.g., 2.4° between K-S and G-T relations), there arises a requirement for an accurate and quantitative method to determine the OR between prior austenite and martensite. However, the situation where scarcely

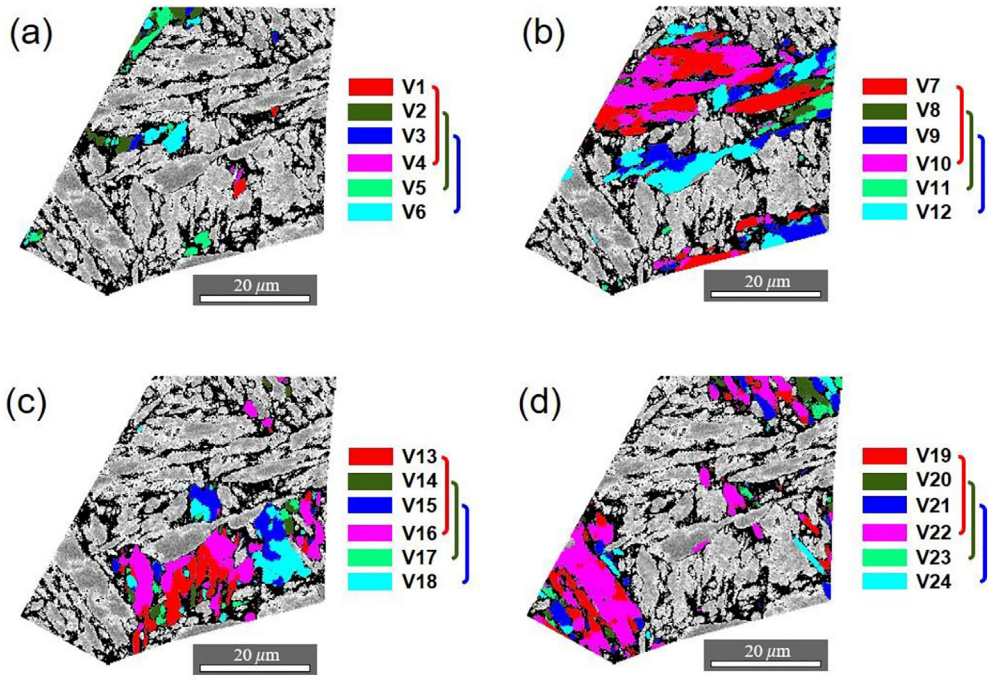


**Fig. 5.** The colored variants showing the blocks with bivariant structure from four crystallographically distinct packets within the prior austenite grain.

retained austenite can be detected constitutes a major obstacle to getting access to the actual OR when it comes to the full lath martensite microstructure. Moreover, even if only a little amount of austenite is retained in the specimen, the orientation of retained austenite always has a deviation from its initial state above $M_S$ temperature, which is caused by the strain accommodation during martensitic transformation. Fortunately, according to the crystallographic theory of martensitic transformation, there is always a reproducible OR for a martensitic steel with a specific composition, which is subject to the mechanism of invariant plane strain. It follows that we can take advantage of it to deduce the OR and OPA by a sufficient number of variants.

In this new approach, the modified K-means clustering algorithm is firstly applied to determine the orientations of variants with their area percentages. Although it seems like an extra calculation, advantages are still obvious: (1) When it comes to the case where there is no condition for variant selection (e.g., the present study), the different area percentages of variants from two-dimensional EBSD analysis is probably caused by a random cross-section of a PAG. It may be, therefore, more reasonable to apply the equally-weighted variants to the optimization scheme of OR and OPA. As shown in the stereographic PFs in Fig. 4 and 8a, the converged variant orientations after clustering indicates a good fit to the experimental data, which therefore is highly representative for the measured data; (2) With respect to the case of variant selection, the present optimization scheme can also consider the area-weighted case through a simple area statistic based on the converged variant orientations. Particularly, due to the good agreement with the measured data, the solution from clustering algorithm shows a higher accuracy than that from previous approach [20] which employs the well-documented ORs, such as K-S OR, to estimate the orientation of variants. It follows that the clustering algorithm has a promising application for the analysis of variant selection; (3) Computational time can be saved significantly through applying the converged variant orientations to the present optimization scheme, since the variant-level data has a prominent advantage in the computation costs compared with the pixel-level data. In addition, although the domain-level calculation is also adopted to save computational time, the accurate orientation information is always lost during the averaging especially for lath martensite steel whose misorientation of V1/V4 is only about 5° [5]. While the variant-level calculation based on the clustering algorithm not only has the highest computational efficiency but also can ensure the accurate information of variant orientations.

In order to obtain the OPA and OR using the variant-level data, a robust optimization scheme is developed. As employed by Beladi [11–13] et al., the criterion of minimizing the SMMA is quite reasonable, and another similar criterion requiring a minimization of the average deviation between measured and predicted data of martensitic orientation was also proposed by Miyamoto [6,14]. However, the fraction of variants serves as an essential role in the variant-level calculation is not involved in their minimization criterion. Following their criterion, an objective function is built in our approach through introducing the variant fraction into Miyamoto's criterion as shown in Eq. (9). Besides that, thanks to the facilities of quaternion, the objective function established using quaternion can be quickly solved by the BFGS quasi-Newton method. As demonstrated above, the least squares fitting method used by

**Table 4**
The solutions of OR and OPA from different methods and the corresponding deviations.

| Method | OR | OPA | $\sum_{m=1}^{N_v} f_m \cdot \Delta\theta_m$ |
|---|---|---|---|
| Area-weighted | $[0.9229, -0.0606, 0.0464, -0.3775]^T$ | $[0.6812, 0.4536, 0.2264, 0.5281]^T$ | 0.4261 |
| Equally-weighted | $[0.9234, -0.0624, 0.0453, -0.3760]^T$ | $[0.6815, 0.4534, 0.2270, 0.5277]^T$ | 0.5461 |
| Humbert's method | $[0.9233, -0.0617, 0.0454, -0.3764]^T$ | $[0.6816, 0.4530, 0.2267, 0.5280]^T$ | 0.5558 |

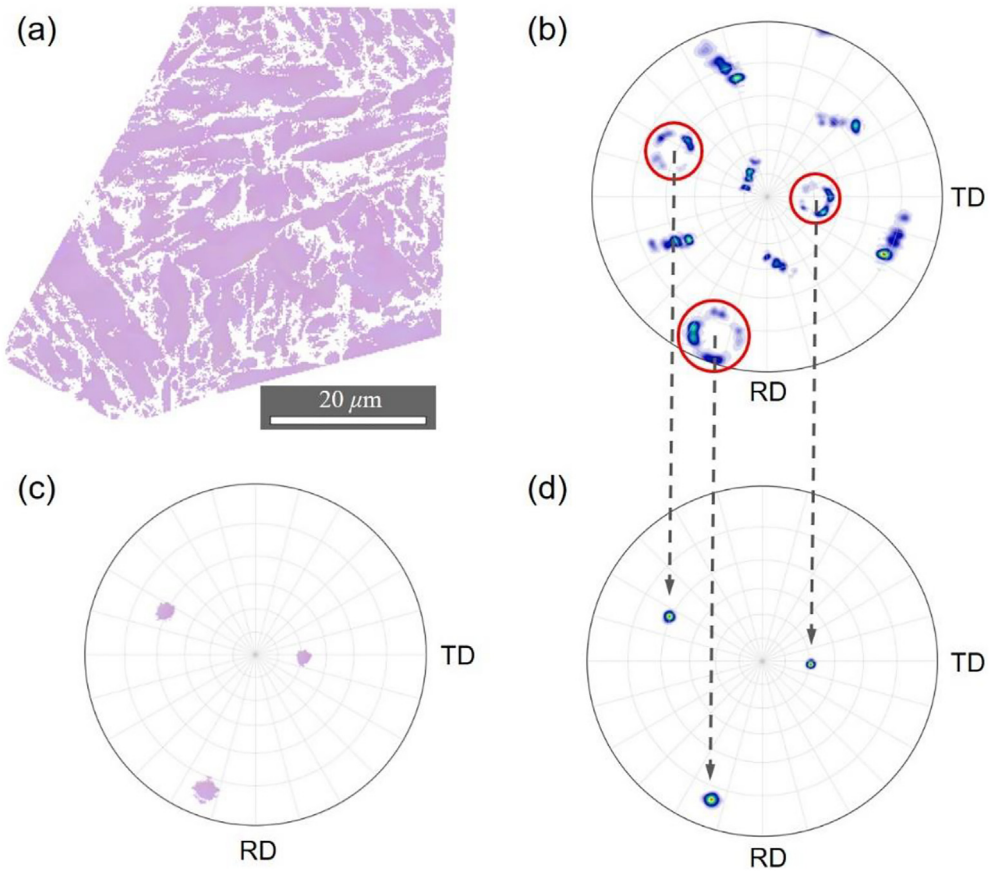


**Fig. 6.** Euler map of reconstructed prior austenite (a) with {001} stereographic pole figures displayed as points (c) and a contour (d); {001} stereographic pole figures of the corresponding lath martensite displayed as a contour (b).

Miyamoto is hard to obtain the optimal solution without numerical calculations [14,30]. It follows that this new approach exhibits a faster calculation speed with equivalent accuracy. Furthermore, although an analytical approach developed by Humbert [15] has the advantage of rapid solution, the solutions from this method cannot always satisfy the minimization criterion in the present study, indicating the lower accuracy as shown in Table 5. Therefore, the high accuracy and efficiency together with an ability of taking variant fraction into consideration are the main merits of this new approach. Recently, there is an increasing attention on the reconstruction of PAGs especially for the ausformed martensite [36–40]. In fact, our new optimization scheme can also be propitious to the reconstruction technique due to the high accuracy and efficiency.

In previous researches, perhaps due to the technology limitation, the solution accuracy was evaluated and verified only based on the experimental data obtained from the retained austenite. Since retained austenite is deformed seriously, it may not be a reliable measurement object. Fortunately, such a crucial difficulty has been overcome in our work by using in-situ HT EBSD examinations. Without the interference of deformation, the orientation data measured from untransformed austenite at high temperature supports our calculation results strongly. That is, our theoretical model has a high accuracy with an error of as low as less than 1°. As we know, the retained austenite undergoes an orientation change after suffering from the transformation strain by the surrounding martensite. Such a deformation induced by transformation can be presented by the kernel average misorientation (KAM) maps recorded at different temperature as shown in Fig. 9. In this case, a higher local misorientation of retained austenite was observed, indicating a larger strain gradient [41]. In fact, as shown in Table 5, the averaged orientation of retained austenite varies from the initial averaged orientation about 1.43°, and the angle becomes even to 3.73° indicated from Fig. 10 when averaging the misorientations between the austenite orientation at each pixel and the initial averaged orientation.

As mentioned above, our new approach will come in handy when no or only a little amount of retained austenite can be observed. In fact, the reason for this phenomenon can be related with the self-accommodation of variants and the hierarchical configuration of lath martensite as displayed in Fig. 5. Recently, Kinney et al. [4] drew a conclusion from a commercial 9 Ni steel that the bivariant blocks (V1/V4 pair) with the invariant planes of $\{011\}_{\alpha'}//\{111\}_{\gamma}$ can be mutually stacked to form a packet without significant internal strain. Once the shear strain can be eliminated effectively through the self-accommodation of bivariant blocks, the austenite is very likely to be fully transformed into martensite after the transformation goes to completion. Indeed, the absence of retained austenite is a common phenomenon especially in nickel steels.

When there is a little amount of retained austenite, it always undergoes an orientation change which may be an inevitable result of transformation strain. From the concept of geometrically necessary dislocations (GND), the higher density of GND indicates the larger gradient of plastic deformation [42,43]. Here, the spatial distribution of GND density is employed to visualize the strain state of the austenite phase. An approximate expression [44,45] of GND density related with local misorientation angle of KAM is specified by Eq. (11):

$$\rho_{GND} \approx 2\theta/bd \tag{11}$$

where $\theta$ (rad) is the misorientation angle of KAM; $b$ is the Burgers vector; $d$ is the step size.

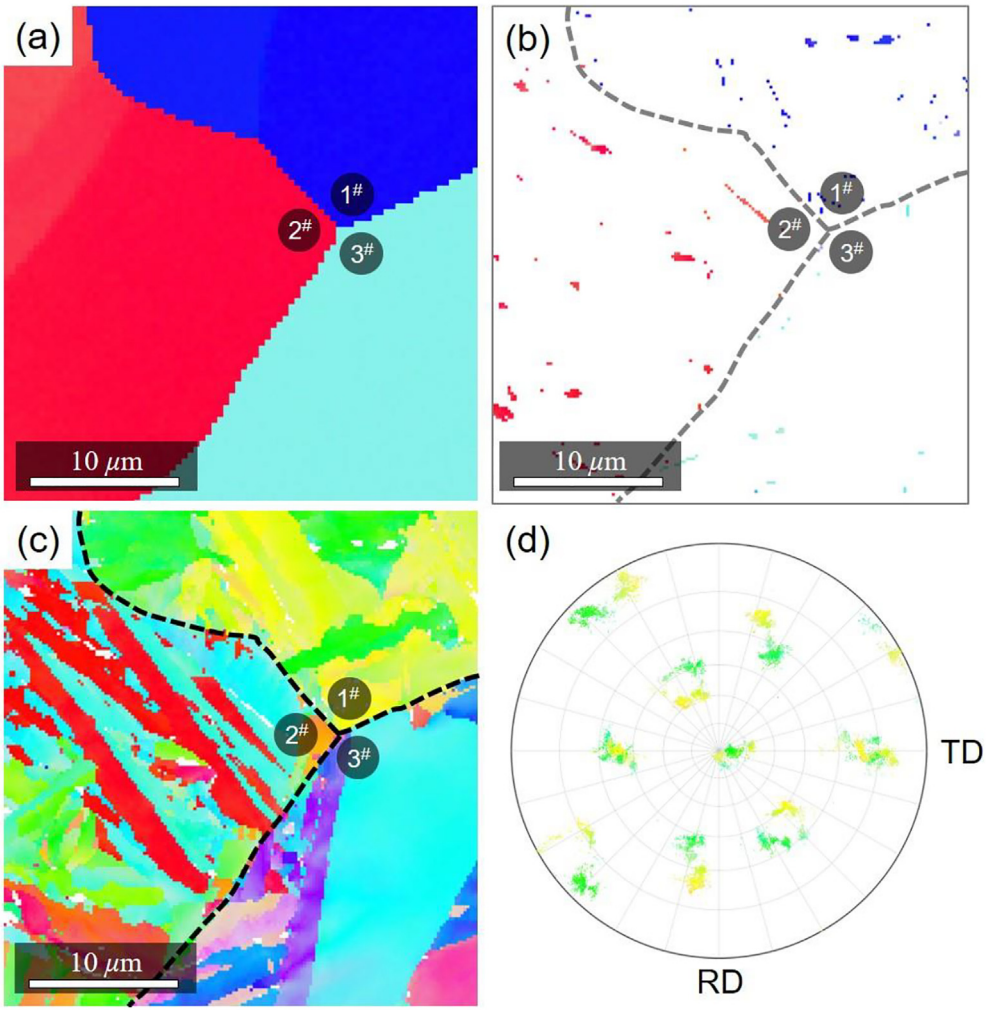


**Fig. 7.** IPF maps of prior austenite at 320 °C (a), retained austenite at room temperature (b), and lath martensite at room temperature (c) with dashed lines indicating the PAG boundaries, and the stereographic PF of martensite within the first PAG (d).

According to the equation above and the data from Fig. 9, the averaged GND density of austenite at 320 °C and room temperature are calculated as $2.30 \times 10^{13}$ $m^{-2}$ and $8.96 \times 10^{13}$ $m^{-2}$ respectively. Such a significant increase in GND density indicates a more serious gradient of plastic deformation and the possibility of orientation change at different positions within a PAG. In addition to the gradient of plastic strain,

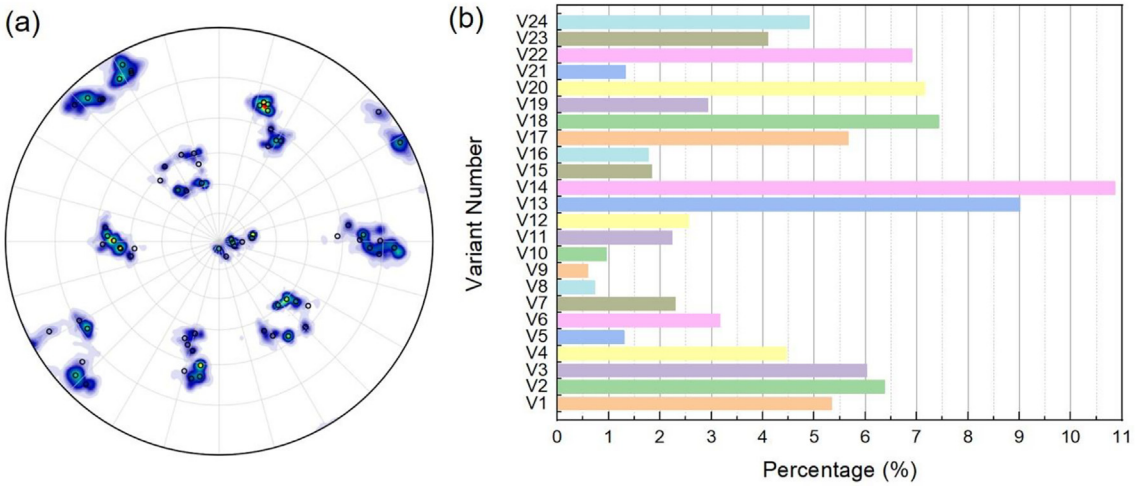


**Fig. 8.** The contoured {011} stereographic PF of martensite within the first PAG superimposed onto the PF of the clustered orientations of variants (a), and the area percentage of each variants after statistic (b).

**Table 5**
The comparison among the averaged orientation of austenite at 320 °C, the OPAs obtained from our new approach, and the averaged orientation of retained austenite at room temperature (RT) with respect to the first PAG.

| | Orientation in quaternion form | Misorientation with the averaged orientation of austenite at 320 °C (°) |
|---|---|---|
| Austenite at 320 °C | $[0.8463, 0.2690, -0.1990, -0.4146]^T$ | – |
| Equally-weighted OPA | $[0.8477, 0.2715, -0.2019, -0.4084]^T$ | 0.8465 |
| Area weighted OPA | $[0.8482, 0.2702, -0.2007, -0.4090]^T$ | 0.7189 |
| Retained austenite at RT | $[0.8411, 0.2665, -0.2053, -0.4236]^T$ | 1.4254 |

the plastic strain itself of retained austenite suffered from the surrounding martensite can be also estimated. According to Ashby's model [43], an approximate relation between the net rotation (i.e., the misorientation of austenite before and after martensitic transformation) and the shear strain is given as:

$$\Delta\theta \approx \varepsilon_\gamma \tag{12}$$

where $\Delta\theta$ is the net rotation (rad), $\varepsilon_\gamma$ is the shear strain, and the equation above is only valid for small $\varepsilon_\gamma$ (less than 0.2). Histogram of the misorientation ($\Delta\theta$) with respect to the first PAG is shown in Fig. 10. And the averaged shear strain derived from Eq. (12) is about 6.5%, which can serve as an important parameter for the crystallographic theory of martensitic transformation. However, it should be noticed that the value of 6.5% may be still underestimated due to the strain relaxation on the surfaces. In fact, the eigen shear strain produced by the formation of a variant is as high as about 24.2% based on the two lattice invariant shears [28]. In turn, the surrounding austenite will undergo the relatively high additional stress. It has been reported recently that dislocation density in retained austenite may be nearly same as in lath

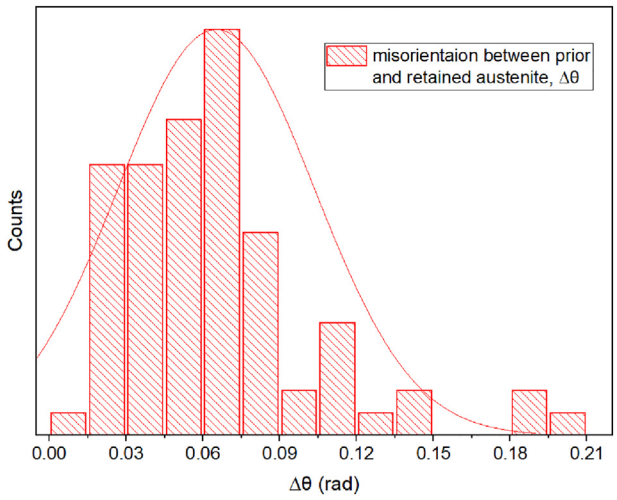


**Fig. 10.** Histogram of the misorientation ($\Delta\theta$) between the initial austenite at 320 °C and the retained austenite at room temperature with respect to the first austenite grain.

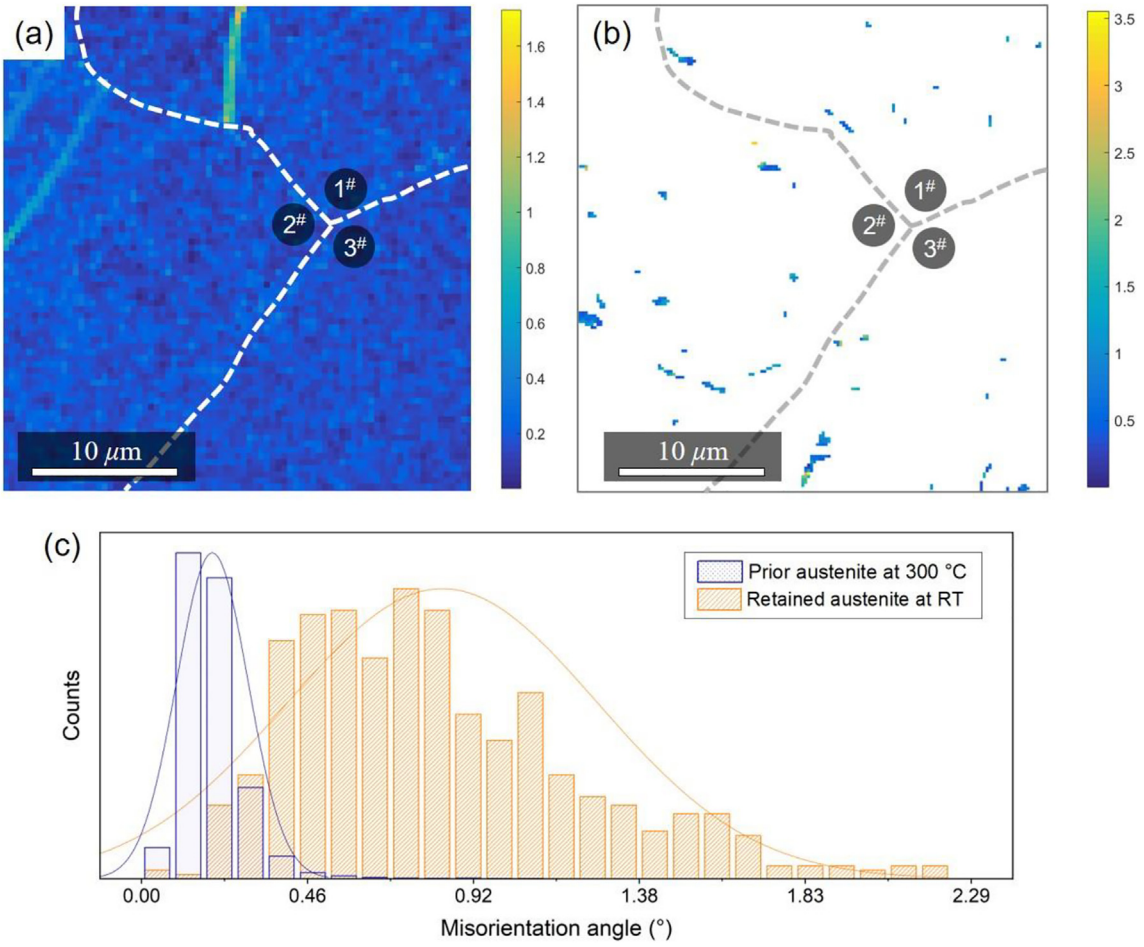


**Fig. 9.** Kernel average misorientation (KAM) maps of prior austenite at 320 °C (a) and the retained austenite at room temperature (b) respectively, where dashed lines indicates the boundaries of PAGs; Histograms of the misorientation angle from the corresponding KAM maps (c).

martensite, such as $5.56 \times 10^{14}\ m^{-2}$ [46]. As a result, the serious plastic strain accompanying with the lattice rotation would occur in retained austenite. Instead of retained austenite at room temperature, the austenite at a temperature near the $M_S$, due to less dislocation interference, is a better candidate to verify the rationality of our approach.

In addition, an interesting result is found that a near G-T OR, instead of the general K-S OR, is obtained from this new approach. it must be related with the crystallographic details during martensitic transformation. One of the notable phenomena for G-T OR is that, the misorientation between two sub-blocks within a block is only 5.72°, rather than the 10.53° for K-S OR. The further crystallographic details about the relationship between OR and mechanical property is now under way and will be reported elsewhere [47].

## 7. Conclusions

In order to overcome the difficulty and inaccuracy in measuring the OR and OPA when there is no enough amount of retained austenite that can be observed in lath martensitic steel at room temperature, a new approach was proposed based on two crucial algorithms: a modified K-means clustering of variant orientations and a robust optimization scheme developed for OR and OPA. The water-quenched Fe-12Ni-1.5Si-0.2C steel was selected to test the effectiveness of this approach under the assistance of in-situ HT EBSD examinations. The following achievements were obtained:

1. The novel approach to determine OR at room temperature excludes the role of retained austenite completely, since a significant orientation change (e.g. >3.5° in average) with respect to the prior austenite surrounded by martensite will lead to an inaccuracy of the actual OR. The experimental verification by in-situ HT EBSD examinations found that the misorientation between the OPA optimized from the variant orientations and the actual examined one above the $M_S$ temperature was less than 1°, indicating that the present approach is more reliable in narrowing the margin of error for OR research.
2. Two factors are responsible for the high solution accuracy in the present approach. The first one is the negligible misorientation between the experimental and the clustered variants according to the orientation comparison from the pole figure analysis, the second one is the robust optimization scheme which strictly satisfies the criterion that a minimum average deviation between the measured and predicted orientation of variant is required. Furthermore, the variant-level calculation, instead of pixel/domain calculation previously used, contributes to the high computational efficiency without scarifying solution accuracy.
3. The clustering algorithm modified and the optimization scheme developed in the present paper are not only the decisive factors for high solution accuracy, the former also have a promising application for the analysis of variant selection, and the later can be also propitious to the reconstruction of austenite grains.

Supplementary data to this article can be found online at https://doi.org/10.1016/j.matdes.2020.109022.

## Declaration of Competing Interest

The authors declare that they have no known competing financial interests or personal relationships that could have appeared to influence the work reported in this paper.

## Acknowledgments

This work was supported by the National Key Research and Development Program of China (Grant No. 2018YFA0702900) and the National Natural Science Foundation of China (Grant No. 51801126). The authors are grateful to Prof. Shipu Chen in Shanghai Jiao Tong University for the valuable discussions during the manuscript preparation.

## Appendix A

The XABX method [30] was designed to apply at the triple junction between three variants for reconstructing the ausformed martensite. And this method is developed based on two assumptions that: i) the OPAs remains the same across the variant boundaries; ii) the local ORs remain close to each other and thus close to a mean OR. In order to match the notations and formulas in the present paper, the XABX method is slightly modified.

For two variants inherited from a PAG:

$$\left[g^D(v_1)\right] = \left[S_j^D(v_1)\right] \cdot \left[\Delta g(v_1)\right] \cdot \left[S_i^P(v_1)\right] \cdot \left[g^P(v_1)\right] \quad (A.\ 1-1)$$

$$\left[g^D(v_2)\right] = \left[S_j^D(v_2)\right] \cdot \left[\Delta g(v_2)\right] \cdot \left[S_i^P(v_2)\right] \cdot \left[g^P(v_2)\right] \quad (A.\ 1-2)$$

where these two variants are represented by $v_1$ and $v_2$ respectively, and the other notations are consistent with the text above. Based on the first assumption of $[g^P(v_2)] = [g^P(v_2)]$, we can obtain the following equation after simple manipulations:

$$\left[g^D(v_2)\right] \cdot \left[g^D(v_1)\right]^{-1} = \left(\left[S_j^D(v_2)\right] \cdot \left[\Delta g(v_2)\right] \cdot \left[S_i^P(v_2)\right]\right) \cdot \left(\left[S_j^D(v_1)\right] \cdot \left[\Delta g(v_1)\right] \cdot \left[S_i^P(v_1)\right]\right)^{-1} \quad (A.\ 2)$$

Then, with the second assumption of $[\Delta g(v_2)] \cong [\Delta g(v_1)] \cong \left[\overline{\Delta g}\right]$, Eq. (A2) can be transformed into:

$$\left[g^D(v_2)\right] \cdot \left[g^D(v_1)\right]^{-1} \cong \left(\left[S_j^D(v_2)\right] \cdot \left[\overline{\Delta g}\right] \cdot \left[S_i^P(v_2)\right]\right) \cdot \left(\left[S_j^D(v_1)\right] \cdot \left[\overline{\Delta g}\right] \cdot \left[S_i^P(v_1)\right]\right)^{-1} \quad (A.\ 3)$$

Next, the term of $\left(\left[S_j^D(v_2)\right] \cdot \left[\overline{\Delta g}\right] \cdot \left[S_i^P(v_2)\right]\right)$ can be replaced by a new term $\left[\overline{\Delta g'}\right]$ for simplifying the notations:

$$\left[g^D(v_2)\right] \cdot \left[g^D(v_1)\right]^{-1} \cong \left[\overline{\Delta g'}\right] \cdot \left(\left[S_j^D(v_1)'\right] \cdot \left[\overline{\Delta g'}\right] \cdot \left[S_i^P(v_1)'\right]\right)^{-1} \quad (A.\ 4)$$

We can further reformulate the Eq. (A. 4) to a general form of $X \cdot A \cong B \cdot X$, where $X$ represents $\left[\overline{\Delta g'}\right]$, $A$ and $B$ are functions of the orientation of variants and of rotational symmetry elements:

$$\left[\overline{\Delta g'}\right] \cdot \left[S_i^P(v_1)'\right]^{-1} \cong \left[g^D(v_2)\right] \cdot \left[g^D(v_1)\right]^{-1} \cdot \left[S_j^D(v_1)'\right] \cdot \left[\overline{\Delta g'}\right] \quad (A.\ 5)$$

The general form of Eq. (A. 5) is where the name of XABX comes from. In order to find an optimal OR, an error function needs be minimized which is established as:

$$E = \|X \cdot A - B \cdot X\|^2 \quad (A.\ 6)$$

with a constraint of $\|X\|^2 = 1$, where $\|\|$ defines the Euclidean norm. It will be very efficient to apply quaternion to resolve this minimization problem, with a new form of $Q_X \cdot Q_A - Q_B \cdot Q_X$ replacing the previous form of $X \cdot A - B \cdot X$. With the quaternion facilities, the quaternion multiplication can be transformed into matrix form:

$$Q_X \cdot Q_A - Q_B \cdot Q_X = R(Q_A) \cdot Q_X - L(Q_B) \cdot Q_X = (R(Q_A) - L(Q_B)) \cdot Q_X \quad (A.\ 7)$$

where the conversion formulas are listed in Eq. (4). Accordingly, the error function can be given by:

$$\|(R(Q_A)-L(Q_B))\cdot Q_X\|^2 = {Q_X}^T\cdot(R(Q_A)-L(Q_B))^T \cdot(R(Q_A)-L(Q_B))\cdot Q_X = {Q_X}^T\cdot S\cdot Q_X \quad (A.\ 8)$$

The minimization of Eq. (A. 8) can solved by introducing a Lagrange multiplier λ with a constrain of $\|Q_X\|^2 = 1$:

$$Min\left({Q_X}^T\cdot S\cdot Q_X+\lambda\left(1-{Q_X}^T\cdot Q_X\right)\right) \quad (A.\ 9)$$

A minimum of Eq. (A. 9) can be reached when the first derivative equal to zero, which means that $S\cdot Q_X = \lambda Q_X$. Hence, we can obtain the minimum value of the error function:

$$Min(E(Q_X)) = Min\left({Q_X}^T\cdot S\cdot Q_X\right) = \lambda \quad (A.\ 10)$$

Accordingly, the eigenvalue λ that is closest to zero of $S$ is retained because it minimizes the error function, and its corresponding eigenvector $Q_X$ determines the solution $X$.

## Appendix B

Given a quaternion $Q = [q_0, q_1, q_2, q_3]^T$ ($q_0$ being the real part, and $q_1$, $q_2$, $q_3$ being the imaginary part), the equivalent right-handed (pre-multiplied) 3 × 3 rotation matrix, $R$, is given by

$$R = \begin{bmatrix} 1-2{q_2}^2-2{q_3}^2 & 2q_1q_2-2q_0q_3 & 2q_0q_2+2q_1q_3 \\ 2q_1q_2+2q_0q_3 & 1-2{q_1}^2-2{q_3}^2 & 2q_2q_3-2q_0q_1 \\ 2q_1q_3-2q_0q_2 & 2q_0q_1+2q_2q_3 & 1-2{q_1}^2-2{q_2}^2 \end{bmatrix} \quad (B.\ 1)$$

The conversion from rotation matrix $R$ to quaternion $Q$ is also given:

$$\begin{cases} q_0 = (1+R[1,1]+R[2,2]+R[3,3])^{1/2}/2 \\ q_1 = (R[3,2]-R[2,3])/4q_0 \\ q_2 = (R[1,3]-R[3,1])/4q_0 \\ q_3 = (R[2,1]-R[1,2])/4q_0 \end{cases} \quad (B.\ 2)$$

## Appendix C

A simple algorithm of reconstructing a PAG is developed, which is to calculate the OPA of each pixel. After obtaining the optimal OR and OPA, we can first confirm the symmetric element of prior austenite and the lath martensite according to Eq. (6)

Then substitute the optimal OR and symmetric elements into Eq. (3), the OPA for each pixel can be determined. After that, the orientation data of prior austenite is changed into the form of Bunge Euler angles, which is further plotted by MTEX 5.1.1 software [22].

## References


[1] T. Maki, Morphology and substructure of martensite in steels, in: E. Pereloma, D.V. Edmonds (Eds.), Phase Transformation in Steels, Woodhead Publishing, Cambridge 2012, pp. 34–58.
[2] L. Qi, A.G. Khachaturyan, J.W. Morris Jr., The microstructure of dislocated martensitic steel: theory, Acta Mater. 76 (2014) 23–39.
[3] C.M. Wayman, Introduction to the Crystallography of Martensite Transformations, The Macmillan Company, New York, 1964.
[4] C.C. Kinney, K.R. Pytlewski, A.G. Khachaturyan, J.W. Morris Jr., The microstructure of lath martensite in quenched 9Ni steel, Acta Mater. 69 (2014) 372–385.
[5] C. Wang, H. Qiu, Y. Kimura, T. Inoue, Morphology, crystallography, and crack paths of tempered lath martensite in a medium-carbon low-alloy steel, Mater. Sci. Eng. A 669 (2016) 48–57.
[6] G. Miyamoto, N. Takayama, T. Furuhara, Accurate measurement of the orientation relationship of lath martensite and bainite by electron backscatter diffraction analysis, Scripta Mater. 60 (2009) 1113–1116.
[7] G. Kurdjumov, G. Sachs, Over the mechanisms of steel hardening, Z. Phys. 64 (1930) 325–343.
[8] Z. Nishiyama, X-ray investigation of the mechanism of the transformation from face centered cubic lattice to body centered cubic, Sci. Rep. Inst. Tohoku Univ. 23 (1934/1935) 637–664.
[9] A.B. Greninger, A.R. Troiano, The mechanism of martensite formation, Metals Trans. 185 (1949) 590–598.
[10] P.M. Kelly, A. Jostsons, R.G. Blake, The orientation relationship between lath martensite and austenite in low carbon, low alloy steels, Acta Metall. Mater. 38 (1990) 1075–1081.
[11] V. Tari, A.D. Rollett, H. Beladi, Back calculation of parent austenite orientation using a clustering approach, J. Appl. Crystallogr. 46 (2012) 210–215.
[12] H. Beladi, G.S. Rohrer, A.D. Rollett, V. Tari, P.D. Hodgson, The distribution of intervariant crystallographic planes in a lath martensite using five macroscopic parameters, Acta Mater. 63 (2014) 86–98.
[13] E. Farabi, P.D. Hodgson, G.S. Rohrer, H. Beladi, Five-parameter intervariant boundary characterization of martensite in commercially pure titanium, Acta Mater. 154 (2018) 147–160.
[14] G. Miyamoto, N. Iwata, N. Takayama, T. Furuhara, Mapping the parent austenite orientation reconstructed from the orientation of martensite by EBSD and its application to ausformed martensite, Acta Mater. 58 (2010) 6393–6403.
[15] M. Humbert, P. Blaineau, L. Germain, N. Gey, Refinement of orientation relations occurring in phase transformation based on considering only the orientations of the variants, Scripta Mater. 64 (2011) 114–117.
[16] Y. Matsuoka, T. Iwasaki, N. Nakada, T. Tsuchiyama, S. Takaki, Effect of grain size on thermal and mechanical stability of austenite in metastable austenitic stainless steel, ISIJ Int. 53 (2013) 1224–1230.
[17] L. Germain, N. Gey, M. Humbert, Reconstruction of deformed parent grains from microstructure inherited by phase transformations, Scripta Mater. 158 (2019) 91–94.
[18] F. Bachmann, R. Hielscher, H. Schaeben, Grain detection from 2d and 3d EBSD data-specification of the MTEX algorithm, Ultramicroscopy 111 (2011) 1720–1733.
[19] Z. Huang, Extensions to the k-means algorithm for clustering large data sets with categorical values, Data Min. Knowl. Disc. 2 (1998) 283–304.
[20] I. Lischewski, G. Gottstein, Nucleation and variant selection during the α-γ-α phase transformation in microalloyed steel, Acta Mater. 59 (2011) 1530–1541.
[21] L. Germain, N. Gey, R. Mercier, P. Blaineau, M. Humbert, An advanced approach to reconstructing parent orientation maps in the case of approximate orientation relations: application to steels, Acta Mater. 60 (2012) 4551–4562.
[22] R. Hielscher, H. Schaeben, A novel pole figure inversion method: specification of the MTEX algorithm, J. Appl. Crystallogr. 41 (2008) 1024–1037.
[23] X.F. Gu, T. Furuhara, W.Z. Zhang, PTCLab: free and open-source software for calculating phase transformation crystallography, J. Appl. Crystallogr. 49 (2016) 1099–1106.
[24] A.G. Khachaturyan, The Theory of Structural Transformations in Solids, John Wiley, New York, 1983.
[25] J.S. Bowles, J.K. Mackenzie, The crystallography of martensite transformations I, Acta Metall. 2 (1954) 129–137.
[26] J.D. Eshelby, The determination of the elastic field of an ellipsoidal inclusion, and related problems, Proc. Roy. Soc. (A) 241 (1957) 241:376.
[27] Y. He, S. Godet, J.J. Jonas, Observations of the Gibeon meteorite and the inverse Greninger-Troiano orientation relationship, J. Appl. Crystallogr. 39 (2006) 72–81.
[28] S. Morito, H. Tanaka, R. Konishi, T. Furuhara, T. Maki, The morphology and crystallography of lath martensite in Fe-C alloys, Acta Mater. 51 (2003) 1789–1799.
[29] H. Kitahara, R. Ueji, M. Ueda, N. Tsuji, Y. Minamino, Crystallographic analysis of plate martensite in Fe-28.5 at.% Ni by FE-SEM/EBSD, Mater. Charact. 54 (2005) 378–386.
[30] M. Humbert, L. Germain, N. Gey, E. Boucard, Evaluation of the orientation relations from misorientation between inherited variants: application to ausformed martensite, Acta Mater. 82 (2015) 137–144.
[31] H. Sato, S. Zaefferer, A study on the formation mechanisms of butterfly-type martensite in Fe–30% Ni alloy using EBSD-based orientation microscopy, Acta Mater. 57 (2009) 1931–1937.
[32] B.K.P. Horn, Closed-form solution of absolute orientation using unit quaternions, J. Opt. Soc. Am. 4 (1987) 629–642.
[33] M. Humbert, N. Gey, J. Muller, C. Esling, Determination of a mean orientation from a cloud of orientations. Application to electron back-scattering pattern measurements, J. Appl. Cryst. 29 (1996) 662–666.
[34] R. Battiti, First-and second-order methods for learning: between steepest descent and Newton's method, Neural Comput. 4 (1992) 141–166.
[35] S. Morito, X. Huang, T. Furuhara, T. Maki, N. Hansen, The morphology and crystallography of lath martensite in alloy steels, Acta Mater. 54 (2006) 5323–5331.
[36] C. Cayron, ARPGE: a computer program to automatically reconstruct the parent grains from electron backscatter diffraction data, J. Appl. Crystallogr. 40 (2007) 1183–1188.
[37] M. Abbasi, T.W. Nelson, C.D. Sorensen, L. Wei, An approach to prior austenite reconstruction, Mater. Charact. 66 (2012) 1–8.
[38] N. Bernier, L. Bracke, L. Malet, S. Godet, An alternative to the crystallographic reconstruction of austenite in steels, Mater. Charact. 89 (2014) 23–32.
[39] M. Kubota, K. Ushioda, G. Miyamoto, T. Furuhara, Analysis of recrystallization behavior of hot-deformed austenite reconstructed from electron backscattering diffraction orientation maps of lath martensite, Scripta Mater. 112 (2016) 92–95.
[40] C.Y. Huang, H.C. Ni, H.W. Yen, New protocol for orientation reconstruction from martensite to austenite in steels, Mater. 9 (2020) 100554.
[41] A. Arsenlis, D.M. Parks, Crystallographic aspects of geometrically-necessary and statistically-stored dislocation density, Acta Mater. 47 (1999) 1597–1611.
[42] N.A. Fleck, G.M. Muller, M.F. Ashby, J.W. Hutchinson, Strain gradient plasticity: theory and experiment, Acta Metall. Mater. 42 (1994) 475–487.

[43] M.F. Ashby, The deformation of plastically non-homogeneous materials, Phil. Mag. 21 (1970) 399–424.
[44] L.P. Kubin, A. Mortensen, Geometrically necessary dislocations and strain-gradient plasticity: a few critical issues, Scripta Mater. 48 (2003) 119–125.
[45] H. Gao, Y. Huang, W.D. Nix, J.W. Hutchinson, Mechanism based strain gradient plasticity I, Theory. J. Mech. Phys. Solids 47 (1999) 1239–1263.
[46] J. Yang, F. Huang, Z. Guo, Y. Rong, N. Chen, Effect of retained austenite on the hydrogen embrittlement of a medium carbon quenching and partitioning steel with refined microstructure, Mater. Sci. Eng. A 665 (2016) 76–85.
[47] D. Sun, Y. Liu, Z. Guo, J. Gu, The microstructure and crystallography of lath martensite with Greninger-Troiano orientation relationship in a Fe-12.8Ni-1.5Si-0.22%C steel [under preparation].